Harmful algal blooms of *Heterosigma akashiwo* (class Raphidophyceae) and environmental features regulate *Mesodinium* cf. *rubrum* abundance in eutrophic conditions

Daniel A. Lemley[a,b*] **(*Corresponding author)**

**To whom all correspondence should be addressed:*

E-mail: DanielAlan.Lemley@mandela.ac.za or lemleydaniel7@gmail.com

ORCID ID: 0000-0003-0325-8499

Janine B. Adams[a,b]

Email: Janine.Adams@mandela.ac.za

Gavin M. Rishworth[b,c]

Email: Gavin.Rishworth@mandela.ac.za

Duncan A. Purdie[d]

Email: duncan.purdie@noc.soton.ac.uk

[a]Botany Department, Nelson Mandela University, Port Elizabeth 6031, South Africa

[b]DSI/NRF Research Chair in Shallow Water Ecosystems, Institute for Coastal and Marine Research (CMR), Nelson Mandela University, Port Elizabeth 6031, South Africa

[c]Zoology Department, Nelson Mandela University, Port Elizabeth 6031, South Africa

[d]Ocean and Earth Science, National Oceanography Centre Southampton, University of Southampton, Southampton SO14 3ZH, United Kingdom

Abstract

Functional drivers of phytoplankton that can potentially form harmful algal blooms (HABs) are important to understand given the increased prevalence of anthropogenic modification and pressure on coastal habitats. However, teasing these drivers apart from other influences is problematic in natural systems, while laboratory assessments often fail to replicate relevant natural conditions. One such potential bloom-forming species complex highlighted globally is *Mesodinium* cf. *rubrum*, a planktonic ciliate. This species occurs persistently in the Sundays Estuary in South Africa yet has never been observed to "bloom" (> 1,000 cell.ml^{-1}). Modified by artificial nutrient-rich baseflow conditions, the Sundays Estuary provides a unique Southern Hemisphere case study to identify the autecological drivers of this ciliate due to artificial seasonally "controlled" abiotic environmental conditions. This study utilised a three-year monitoring dataset (899 samples) to assess the drivers of *M.* cf. *rubrum* using a generalised modelling approach. Key abiotic variables that influenced population abundance were season and salinity, with *M.* cf. *rubrum* populations peaking in summer and spring and preferring polyhaline salinity regions (>18) with pronounced water column salinity stratification, especially in warmer months. This was reflected in the diel vertical migration (DVM) behaviour of this species, demonstrating its ability to utilise the optimal daylight photosynthetic surface conditions and high-nutrient bottom waters at night. The only phytoplankton groups clearly associated with *M.* cf. *rubrum* were Raphidophyceae and Cryptophyceae. Although *M.* cf. *rubrum* reflects a niche overlap with the dominant HAB-forming phytoplankton in the estuary (the raphidophyte, *Heterosigma akashiwo*), its reduced competitive abilities restrict its abundance. In contrast, the mixotrophic foraging behaviour of *M.* cf. *rubrum* exerts a top-down control on cryptophyte prey abundance, yet, the limited availability of these prey resources (mean < 300 cells ml^{-1}) seemingly inhibits the formation of red-water accumulations. Hydrodynamic variability is necessary to ensure that no single phytoplankton HAB-forming taxa outcompetes the rest. These results confirm aspects of the autecology of *M.* cf. *rubrum* related to salinity associations and DVM behaviour and contribute to a global understanding of managing HABs in estuaries.

Keywords: Cryptophytes; eutrophication; *Heterosigma akashiwo*; phytoplankton; planktonic ciliates

1. Introduction

Estuaries are focal points for human settlement due to the abundant ecosystem services they provide. Occupying the dynamic land-sea interface, estuaries have unique physical, chemical and biological characteristics and processes, which translates into productive but naturally stressed environments that are susceptible to perturbations (Paerl et al., 2014; Cloern et al., 2016). The effects of anthropogenic disruptions are compounded in microtidal systems compared to well-flushed macrotidal estuaries due to increased water retention times and high accumulation potential (Warwick et al., 2018; Adams et al., 2020). Increased nutrient loading, hydrological modifications and climatic shifts are at the forefront of anthropogenically-driven global change pressures that threaten the ecological condition and sustainability of estuaries. Continued eutrophication from accelerated nitrogen (N) and phosphorus (P) loading has led to increasing occurrences of undesirable disturbances globally. One example is the increased frequency, magnitude and geographic extent of harmful algal bloom (HAB) proliferations. These HABs can be categorised as either toxic (e.g. shellfish poisoning, bioaccumulation) or non-toxic (e.g. oxygen depletion, reduced light penetration, loss of nursery function, food-web restructuring), with the latter typically associated with prolonged high-biomass accumulations associated with eutrophication (Anderson, 2009). The role of modern global change pressures (e.g. nutrient loading, climate shifts) in the expansion and severity of HABs is convincing (Glibert, 2020). Yet, autecological studies that underscore the abiotic and biotic interactions facilitating the occurrence of HAB species are scarce, despite how necessary these are to inform management efforts that aim to limit detrimental ecological (e.g. loss of biodiversity and natural ecosystem functionality) and economic (e.g. increased monitoring costs, aquaculture and commercial fisheries losses) consequences of these phenomena (Glibert, 2017, 2020; Qin and Shen, 2017; Lemley et al., 2018a).

Mesodinium represents a genus of ciliates (Phylum Ciliophora) that are widely distributed globally in coastal and estuarine environments. The mixotrophic *M. rubrum* (Lohman, 1908; Class Litostomatea) (formerly *Myrionecta rubra* Jankowski, 1976) species has received much attention, particularly since the 1980s (Lindholm, 1985; Crawford, 1989), due to its ability to acquire phototrophy through capturing free-living cryptophyte prey (Gustafson et al., 2000; Johnson et al., 2007). This process entails the sequestration of organelles (e.g. plastids,

mitochondria) which, once acquired through feeding, reside in a quasisymbiotic state that enables pigment synthesis, plastid division and cell division in *M. rubrum* (Johnson, 2011). However, the continued replenishment of prey nuclei is required – a process referred to as karyoklepty – for these processes to be maintained at maximum rates (Johnson et al., 2007). These transcriptionally active nuclei allow for *M. rubrum* to control photosynthetic growth and enable photoacclimation processes for several weeks, after which the nuclei become diluted (~up to 30 days) and population growth declines (Johnson et al., 2007; Herfort et al., 2011b; Peterson et al., 2013; Lasek-Nesselquist et al., 2015; Peltomaa and Johnson, 2017; Moeller and Johnson, 2018; Altenburger et al., 2020).

Despite *M. rubrum* often reported as the sole constituent of the genus, numerous cryptic species exist. Six estuarine/marine species of *Mesodinium* have been described and can be grouped according to habitat preference (benthic or pelagic) and nutritional mode (heterotrophic or phototrophic) (Hansen and Fenchel, 2006; Hansen et al. 2013; Johnson et al., 2016; Moeller and Johnson, 2018; Nishitani and Yamaguchi, 2018; Kim and Park, 2019). For example, the pelagic mixotrophs *M. major* and *M. rubrum* are characterised by predominantly acquired phototrophic behaviour (>95% of carbon acquired from photosynthesis) and specialist feeding on the *Teleaulax*/*Plagioselmis*/*Geminigera* [TPG] clade of cryptophytes, with the only distinction being the increased size and slight morphological differences observed in *M. major* (e.g. more chloroplasts and mitochondria). A more generalist approach to prey specificity, adoption of both phototrophic and heterotrophic nutritional strategies, and a lack of acquired nuclei characterise the benthic *M. chamaeleon* and *M. coatsi*, while *M. pulex* and *M. pupula* are strict heterotrophs lacking plastid sequestration.

Mesodinium cf. *rubrum* populations have a well-documented tendency to form non-toxic HABs (> 1 x 10^3 cells ml^{-1}) that can discolour the water red in temperate estuaries. Such red-tide events, for example, have been reported in North America (Herfort et al., 2011a, 2011b, 2012; Johnson et al., 2013; Peterson et al., 2013) and Europe (Crawford et al., 1997; Pereira et al., 2012). Given its tolerance of a large salinity and temperature range, other factors such as nutrient and light availability, or increased water column stability (e.g. established vertical salinity and temperature gradients), tend to promote the abundance of *M.* cf. *rubrum*. As such, the ability of this

103 species to dominate phytoplankton communities can be attributed to its high motility (up to 1.2 cm s^{-1}), diel
104 vertical migration (DVM) behaviour, rapid nutrient uptake (ammonium and nitrate), and osmotrophic
105 capabilities (DON uptake) (Crawford et al., 1997; Fenchel and Hansen, 2006; Hansen et al., 2013; Johnson et al.,
106 2013; Lemley et al., 2018a). In South Africa, *M*. cf. *rubrum* occurs in the agriculturally influenced Sundays
107 Estuary that is characterised by constant nutrient-rich freshwater inflows and a stable hydrodynamic
108 environment (Lemley et al., 2018a, 2018b). However, high-biomass proliferations of *M*. cf. *rubrum* are largely
109 absent in the system despite the availability of cryptophyte prey and a seemingly suitable environment. A fine-
110 scale study by Lemley et al. (2018a) hypothesised that the prevalence of other persistent HAB species (e.g.
111 *Heterosigma akashiwo*; Class Raphidophyceae), with less complex resource requirements for growth, may limit
112 the bloom magnitude of *M*. cf. *rubrum* in the Sundays Estuary. Here, we have compiled data collected during
113 various monitoring programs beyond that of previous assessments (Lemley et al., 2018a, 2018b) to address the
114 proposed hypothesis that a combination of abiotic factors and co-occurring phytoplankton classes shape the
115 autecology of *M*. cf. *rubrum*. The dynamics between *M.* cf. *rubrum* ciliates and other HAB-forming species,
116 such as *H. akashiwo*, is not well-understood. As such, the well-monitored Sundays Estuary provides the ideal
117 case study from which to delve into the autecology of *M*. cf. *rubrum*, with the overall objective of providing
118 information that can aid the effective mitigation of HABs.
119
120 **2. Materials and Methods**
121
122 ***2.1. Study area***
123 The Sundays Estuary is a predominantly open microtidal system situated along the warm temperate south coast
124 of South Africa. Permanent marine connectivity with the Indian Ocean is maintained through a narrow,
125 meandering estuarine mouth inlet (33°43'17.89"S; 25°51'13.48"E), which facilitates semidiurnal tidal exchanges.
126 The estuary is 24 km in length and is characterised by shallow water depths (~2 m) and a channel-like
127 morphology; see Lemley et al. (2017, 2018b) for study site maps. Given the shallow nature of the estuary, light
128 is considered a non-limiting factor to the growth of phytoplankton, with photic depths (Z_p) typically near to or
129 exceeding water column depths (Table 1). Numerous studies have documented the permanent state of eutrophy

in the Sundays Estuary (Kotsedi et al., 2012; Lemley et al., 2017, 2018a, 2018b), which stems from extensive agricultural activities (e.g. citrus cultivation) and an interbasin water transfer scheme in its upstream catchment. These activities have dampened hydrodynamic variability in the estuary and culminated in a highly stable environment subject to constant nutrient-rich baseflows (~nitrate and phosphate). This lack of natural dynamism has enabled the persistence of numerous HAB species (e.g. *Heterosigma akashiwo*, *Heterocapsa rotundata*) that drive seasonal bottom-water hypoxia in the estuary during the decay of high-biomass accumulations (> 500 µg Chl-*a* l^{-1}) (Lemley et al., 2017).

Table 1. Photic depth variability in relation to water column depths in the Sundays Estuary. Secchi depth (m) measurements were used to calculate photic depth (Z_p, m) according to equations prescribed by Cole and Cloern (1987).

Sampling periods	*n*	Water depth (m)	Photic depth, Z_p (m)	Mean proportion of water column with light (%)	Reference
January-December 2015	66	1.0 – 4.0	0.8 – 3.1	83.6	Lemley et al., 2017
July 2016	10	1.8 – 2.4	2.1 – 3.1	100	-
November 2016	10	1.6 – 2.5	1.1 – 3.0	95.4	Lemley et al., 2018b
April 2018	6	1.2 – 2.6	2.6 – 3.6	100	-
November 2019	8	1.5 – 2.5	1.8 – 3.6	98.7	-

2.2. Data sources

Abiotic and phytoplankton data, including *Mesodinium* cf. *rubrum* abundance, was sourced from numerous research programmes in the Sundays Estuary. The dataset encompasses observations over three years (i.e. 2016, 2018 and 2019) and includes 50 sampling intervals (~49 discrete dates due to an overlap in October 2018), with a total of 899 explicit samples across multiple sampling localities and depths. The sampling design during the study period varied spatially according to the specific research objectives. A near continuous monthly monitoring dataset (excluding May–July 2018), that encompassed oligohaline (> 0.5) to mixoeuhaline (> 30) waters, was available from April 2018 to November 2019 (*n* = 16). Additionally, and with a focus on mesohaline (5–18) and polyhaline (18–30) waters, intensive biweekly datasets (*n* = 34) were available for 2016 (July/August and October/December) and 2018 (October/November). Together, the data are representative of all seasons. The

known recurrent nature of seasonal HABs in the Sundays Estuary (Lemley et al., 2017) is reflected by increased sampling intervals in spring (n = 28; 56% of all samples) and winter (n = 13; 26%) compared to other seasons (10% and 8% for autumn and summer, respectively). Moreover, a total of 27 sampling dates (August 2018 to July 2019) include both day and night data to assess the DVM behaviour of flagellated phytoplankton classes.

Methods for abiotic and phytoplankton collection have been described previously (Lemley et al. 2018a, 2018b). All parameters were assessed concomitantly at 0.5 m water depth intervals, i.e. surface (0 m), 0.5 m, 1 m and at the bottom of the water column (mean depth: 1.88 ± 0.65 m; range: 1.2 to 4 m). Salinity, temperature (°C), dissolved oxygen (mg l^{-1}) and pH were recorded *in-situ* using either a HANNA HI98194, YSI ProDSS or YSI 6600-V2 multiparameter meter. Water samples for laboratory analysis were collected using a weighted pop-bottle. For inorganic nutrient analyses, samples were filtered onboard through hydrophilic polyvinylidene difluoride (PVDF) 0.47 µm pore-size syringe filters, and subsequently frozen. Orthophosphate (PO_4^{3-}), ammonium (NH_4^+) and total oxidised nitrogen (NO_x, i.e. $NO_3^- + NO_2^-$) concentrations were determined using a SEAL AutoAnalyzer 3 HR (SEAL Analytical, Inc.) or standard spectrophotometric methods (Bate and Heelas, 1975; Parsons et al., 1984). Nutrient detection limits were similar for the standard spectrophotometric (PO_4-P = 0.23 µM; NH_4-N = 0.78 µM; NO_x-N = 0.91 µM) and automated (PO_4-P = 0.19 µM; NH_4-N = 0.23 µM; NO_x-N = 0.97 µM) analysis methods. To determine phytoplankton biomass (chlorophyll-*a* concentration), replicates of a known volume of water were filtered through 1.2 µm pore-size glass fibre filters (Munktell© MGC) and frozen before analysis. Thawed filters were placed into glass vials with 10 ml of 95% ethanol (Merck© 4111) for 24 hours in a cold (~2°C), dark room to allow for extraction. Subsequently, chlorophyll-*a* concentrations of refiltered extracts were determined according to Nusch (1980) using a Thermo Scientific™ GENESYS™ 10S UV-Vis spectrophotometer. Water collected for phytoplankton identification and enumeration was fixed with 25% glutaraldehyde solution (Sigma-Aldrich® Chemicals G5882) to a final concentration of 1% (by volume). The Utermöhl method was used to settle a known volume of sample (Coulon and Alexander, 1972), before conducting cell counts using an inverted Leica DMIL phase contrast microscope at 630X magnification. Cells were grouped according to phytoplankton classes, i.e. Bacillariophyceae, Chlorodendrophyceae, Cryptophyceae,

Dinophyceae, Euglenophyceae, Raphidophyceae, and *Mesodinium* cf. *rubrum*. Lastly, abundance (cells ml^{-1}) was calculated using the equation described by Snow et al. (2000).

2.3. Data analysis

Only those sampling occasions that represented a complete suite of all possible predictor variables measured were considered in relation to *Mesodinium* dynamics, thereby reducing the dataset to 795 explicit samples across 204 localities (multiple depths sampled at each) from April 2018 to November 2019 (28 sampling days in total). Incomplete datasets omitted from the model included the winter (~nutrients) and spring (~pH) biweekly sampling in 2016, as well as a single sampling day from the 2018 biweekly sampling (i.e. 1 November; ammonium not recorded). Each included sample in the model was treated as spatially independent given the known properties of the Sundays Estuary water column in terms of residence time relative to tidal cycles (Lemley et al. 2018a, 2018b).

Mesodinium abundance (cells ml^{-1}) was modelled in relation to measured biotic and abiotic variables using the 'nlme' package in R (Pinheiro et al. 2018; R Core Team, 2020). Predictor variables measured *in situ* (see above) and considered were: phytoplankton class (Bacillariophyceae, Chlorodendrophyceae, Cryptophyceae, Dinophyceae, Euglenophyceae and Raphidophyceae) and total log(x+1) biomass, nutrient concentrations (total oxidised nitrogen, ammonium, phosphate), physico-chemistry (dissolved oxygen, temperature, salinity, pH), diel state (day versus night), sampling depth (from surface in 0.5 m increments up to 1.0 m, and including a bottom sample), vertical salinity and temperature stratification (difference between bottom and surface water), as well as the interaction of this, and the date of sampling. To assess the importance of DVM in relation to *Mesodinium*, the interaction between diel state and depth was also included as a predictor. All numerical (non-factorial) factors were scaled prior to analysis to allow for standardised comparisons between model coefficients (Zuur et al. 2009). Correlation (r) estimates and variance inflation factors (VIFs) were calculated amongst all predictor variables and those which were colinear ($r > 0.6$ or $VIF > 4.0$) were not considered further (Zuur et al. 2009, 2010).

The optimal random residual variance structure was determined by comparing ('anova', using likelihood ratio tests; all models fitted under restricted maximum likelihood: REML) a null linear model fitted with all possible predictors with separate GLS or linear mixed-effects (LME) models that incorporated all possible combinations of correlation ('date' considered as a temporal autocorrelation 'corAR1' structure), variance ('season' considered as an identity structure) and random ('season' considered) structures (Zuur et al. 2009, 2010). The optimal random structure included 'season' as a variance identity weighting and 'date' as a temporal autocorrelation structure; from this a GLS model was fitted under maximum likelihood (ML) with all predictor variables. The most-parsimonious version of this model was determined through model selection using Akaike Information Criterion (AIC) scores, comparing each full model to sequential single-term deletions until $\Delta AIC < 0.5$ (Zuur et al. 2009). This most-parsimonious model was then refit under REML estimation and the coefficients of each term assessed using 'anova' or 'summary' statistics (Zuur et al. 2009). Using these most-parsimonious predictors, two seasonal models were also fitted under REML estimation, using subset data from spring or summer and autumn or winter.

3. Results

Of the 899 samples, 508 (56.5%) recorded *M.* cf. *rubrum* during the study period (Table 2), indicating the resident nature of this species in the Sundays Estuary plankton community. Samples comprised predominantly mesohaline (54.1%) and polyhaline (35.6%) salinity regions, although few were oligohaline (4.9%) and mixoeuhaline (5.5%). Cell concentrations of *M.* cf. *rubrum* never exceeded the threshold typically associated with red-tide accumulations (> 1000 cells ml^{-1}; Crawford et al., 1997). The highest cell abundance recorded was 807 cells ml^{-1}, and "bloom" levels exceeding 100 cells ml^{-1} (Johnson et al., 2013) were observed in 10.6% of the total samples.

The ubiquitous nature associated with *M.* cf. *rubrum* was evidenced by its occurrence (n = 508) in broad salinity (17.6 ± 7.1) and temperature (20.9 ± 3.2°C) ranges during the study period (Table 2). Water that was more saline (t = 2.4; $P < 0.05$) and especially where there was a pronounced vertical salinity gradient between surface and

bottom water (t = 2.7; P < 0.01) corresponded with higher *M*. cf. *rubrum* abundance (Table 3). This is demonstrated by the unimodal peak observed along the salinity gradient (Fig. 1) and "bloom" concentrations occurring in predominantly polyhaline regions (18.8 ± 5.5) with enhanced stratification (Δ Salinity: 11.9 ± 3.9) (Fig. 2 and Table 2). Contrastingly, thermal stratification between surface and bottom-waters had no notable effect on the abundance of *M*. cf. *rubrum* overall (Table 3, P > 0.2). Yet, the seasonal spring/summer GLS model suggested that *M*. cf. *rubrum* marginally favoured (P < 0.10) the cooler surface waters in spring compared to the well-established thermoclines typical of the summer months. Season was also identified as an important predictor variable in the most parsimonious model explaining *M*. cf. *rubrum* population dynamics (Table 3, P < 0.05), indicating peak abundance and highest residual variability in summer followed by spring. However, the bimodal temperature distribution pattern (Fig. 1) and the exclusion of water temperature as a predictor variable in the most parsimonious GLS model suggests that other seasonally distinct variables drive this observation.

An increasing abundance of *M*. cf. *rubrum* coincided with well-oxygenated, less variable (Table 2), water column conditions (5–9 mg l^{-1}), with declines observed during hypoxic (< 3 mg l^{-1}) and super-saturated (> 10 mg l^{-1}) dissolved oxygen conditions (Fig. 1). Similarly, more acidic conditions corresponded with increases in *Mesodinium* concentrations (t = -3.0, P < 0.01; Table 3). Accordingly, *Mesodinium* concentrations exhibited marked reductions in conjunction with more basic environments (pH > 9) that are typically associated with high-biomass phytoplankton accumulations (~photosynthetic activity) (Fig. 1). A positive relationship was identified between *M*. cf. *rubrum* abundance and phytoplankton biomass (t = 2.9, P < 0.01; Table 3), with concentrations peaking in meso- to eutrophic conditions (≥ 5 but < 60 µg Chl-*a* l^{-1}; $\log_{(x+1)}$: 0.8–1.9). However, the onset of high-biomass phytoplankton bloom events (> 100 µg Chl-*a* l^{-1}; $\log_{(x+1)}$ = 2.0; n = 87) signalled a drop in *Mesodinium* cell concentrations (Fig. 1). This pattern is illustrated by the phytoplankton biomass levels that characterise "bloom" (28.7 ± 43.8 µg Chl-*a* l^{-1}) and "absence" (57.1 ± 100.3 µg Chl-*a* l^{-1}) periods of *M*. cf. *rubrum* in the Sundays Estuary (Table 2).

Inorganic nutrient concentrations recorded in this study reflected the nutrient-rich conditions previously reported for the Sundays Estuary (Lemley et al., 2017, 2018a, 2018b). More specifically, the observed ranges of total

oxidised nitrogen (NO_x-N: 0 to 82.7 µM) and phosphate (PO_4-P: 0 to 10.0 µM) highlight the influence of catchment agricultural activities. Of these, only phosphate was included as one of the most parsimonious predictors in the GLS model and showed a weakly positive overall correlation with *M*. cf. *rubrum* abundance, (P = 0.2), but especially pronounced in the cooler seasons (Table 3, $P < 0.05$). This equated to a largely unimodal peak when assessing the occurrence of *M*. cf. *rubrum* (n = 508) in relation to phosphate concentrations (Fig. 1), displaying a central tendency of 1.7 ± 1.2 µM. Total oxidised nitrogen (11.2 ± 15.2 µM) and ammonium (2.6 ± 3.8 µM) lacked any clear relationship with *Mesodinium* abundance during this study (Fig. 1), although being observed in waters with predominantly low dissolved inorganic nitrogen concentrations (< 10 µM) (Table 2).

Table 2. Abiotic and phytoplankton characteristics associated with varying population densities of *M.* cf. *rubrum* in the Sundays Estuary.

	Absent (0 cells ml^{-1})		**Low (< 100 cells ml^{-1})**		**"Bloom" (> 100 cells ml^{-1})**	
	Mean	***SD***	***Mean***	***SD***	***Mean***	***SD***
Salinity	14.1	8.4	17.3	7.4	18.8	5.5
Temperature (°C)	20.4	3.5	20.9	3.3	21.0	3.1
Dissolved oxygen (mg l^{-1})	8.1	3.3	7.4	2.9	7.5	2.4
pH	8.6	0.4	8.6	0.4	8.5	0.4
Chlorophyll-*a* (µg l^{-1})	57.1	100.3	30.3	50.7	28.7	43.8
PO_4-P (µM)	1.5	0.9	1.7	1.2	1.7	1.4
NO_x-N (µM)	14.9	17.7	8.4	12.0	8.0	12.5
NH_4-N (µM)	2.4	3.0	2.8	4.2	3.0	4.8
Stratification (Δ Salinity)	8.7	5.8	10.0	5.1	11.9	3.9
Phytoplankton classes (cells ml^{-1})						
Bacillariophyceae	630	1,719	530	1,582	821	1,594
Chlorodendrophyceae	195	460	254	485	203	357
Cryptophyceae	283	1,083	95	161	148	189
Dinophyceae	531	934	434	1,034	511	1,060
Euglenophyceae	13	53	17	74	31	88
Raphidophyceae	2,777	7,249	856	3,052	868	3,463
Samples [*n* (%)]	391 (43.5)		413 (45.9)		95 (10.6)	

Distinct vertical distribution of *M.* cf. *rubrum* cells were observed throughout the water column ($P < 0.001$; Table 3), with surface water concentrations (in the order: 1 m > 0.5 m > 0 m, overall) higher than those observed in bottom-waters, particularly during the day-time (Fig. 2). *M*. cf. *rubrum* was most abundant at mid-range waters in autumn/winter and surface waters in spring/summer (Table 3). No notable differences were observed in *M.* cf. *rubrum* abundance between day versus night samples overall (P = 0.3; Table 3). In terms of DVM fluctuations, *M*. cf. *rubrum* populations indicated a distinct preference for bottom-waters at night, particularly in spring/summer ($P < 0.05$; Table 3). This night-time accumulation in bottom-waters occurs at varying degrees of salinity stratification (Fig. 2). Contrastingly, accumulation in the surface waters is amplified by more prominent vertical salinity gradients during the day, particularly during the warmer seasons ($t = 4.0$; $P < 0.001$; Table 3). Despite its omittance from the modelled subset, these same patterns of depth and diel cycle variations were also identified for *Mesodinium* in datasets collected in 2016 (Lemley et al., 2018a, 2018b).

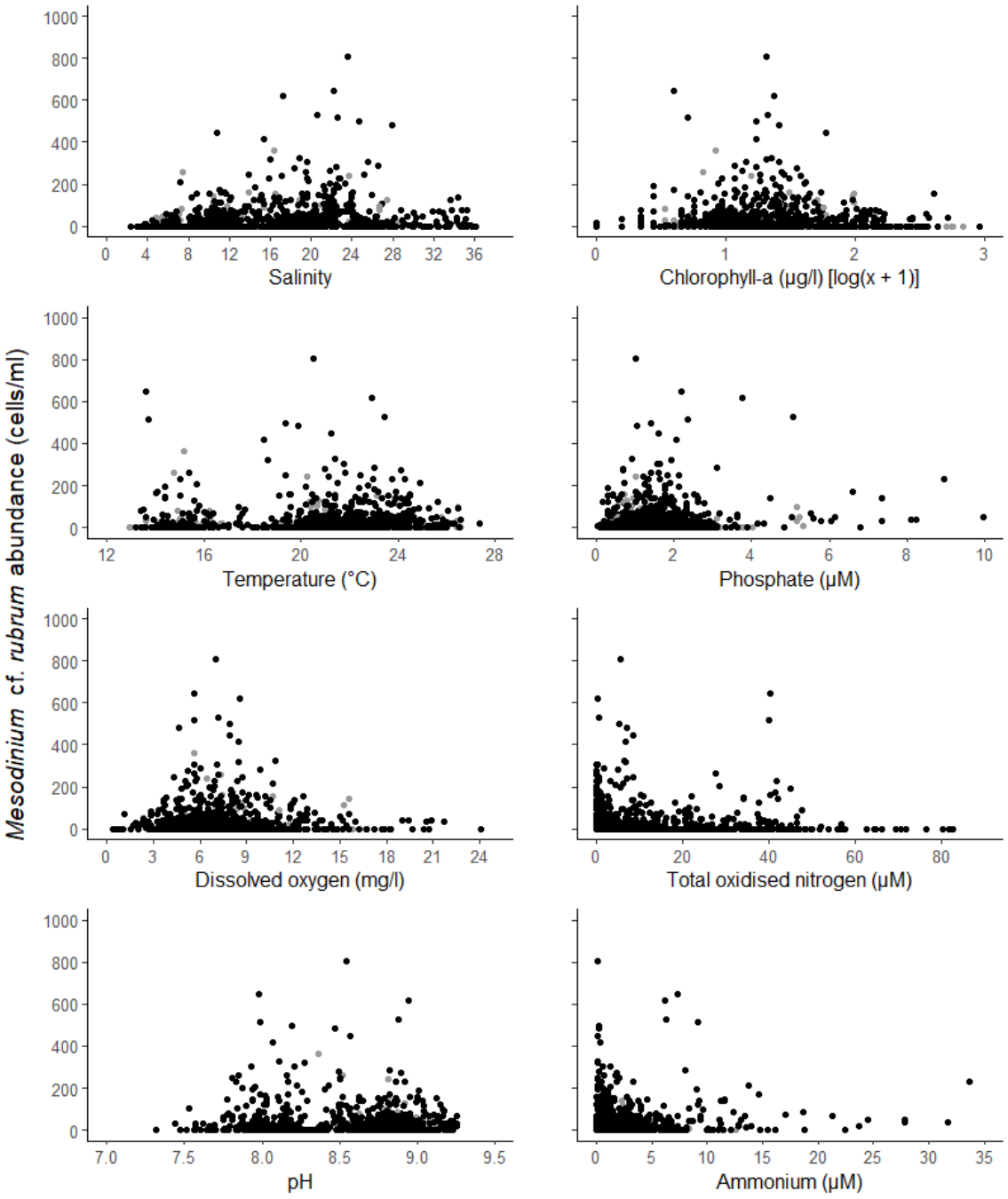

Figure 1. *Mesodinium* cf. *rubrum* abundance (y-axis) versus salinity, temperature, dissolved oxygen, pH, phytoplankton biomass (chlorophyll-*a*) and inorganic nutrients (phosphate, total oxidised nitrogen and ammonium). Black points indicate modelled subset data (n = 795) and grey points indicate sampling occasions with incomplete datasets ($n \leq 104$).

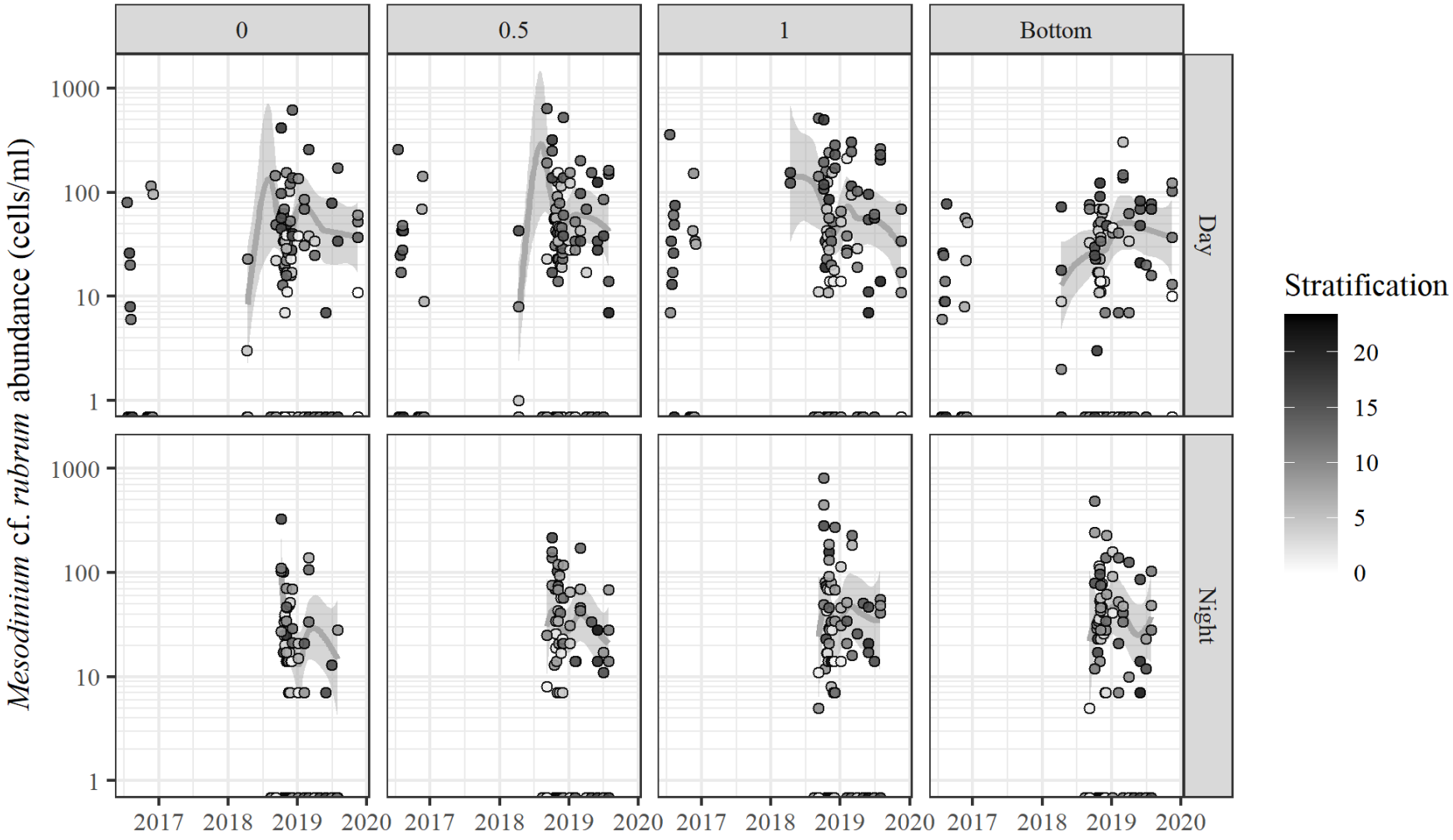

Figure 2. Temporal distribution of *M.* cf. *rubrum* abundance in the Sundays Estuary, South Africa, relative to sampling depth and diel state (day versus night). Abundance values are colour-coded according to salinity stratification, this being the difference in salinity between bottom and surface waters. A 'loess' smoother line (±SE) is drawn for those data that are included in the modelled subset (see 'Data analysis': April 2018 to November 2019).

292 The permanently eutrophic condition of the Sundays Estuary was highlighted by 40.8% of the sampling intervals
293 (n = 20) exhibiting high-biomass phytoplankton accumulations (> 100 µg Chl-*a* l^{-1}). Of these, the majority
294 (70%) represented nearly monospecific and high density (> 5,000 cells ml^{-1}; max. 69,968 cells ml^{-1}) HABs of *H.*
295 *akashiwo* (Class Raphidophyceae). The remaining high-biomass instances comprised bloom events of species
296 belonging to the following phytoplankton classes: Bacillariophyceae (*Pleurosigma angulatum*, max. 1,759 cells
297 ml^{-1}; n = 3), Cryptophyceae (*Plagioselmis nannoplanctica*, max. 15,551 cells ml^{-1}; n = 1), and Dinophyceae
298 (unidentified species belonging to the Order Peridiniales, max. 4,897 cells ml^{-1}; n = 2). The interactions between
299 *M*. cf. *rubrum* and co-occurring phytoplankton classes were assessed in the GLS model. The strongest
300 interaction was observed with Raphidophyceae, where higher *H. akashiwo* abundance corresponded with low *M.*
301 cf. *rubrum* abundance (t = -2.2, P < 0.05; Fig. 3 and Table 3), particularly in the warmer months (t = -2.4). This
302 relationship is further evidenced by the abundance of Raphidophyceae associated with "absence" (2,777 ± 7,249
303 cells ml^{-1}) and "bloom" (868 ± 3,463 cells ml^{-1}) periods of *Mesodinium* (Table 2). Notably, *Mesodinium*
304 abundance was largely unaffected (P = 0.4) by *H. akashiwo* populations during the cooler autumn and winter
305 months. Additionally, model results highlighted an overall inverse relationship between *M*. cf. *rubrum*
306 abundance and its Cryptophyceae prey source (t = -1.8, P < 0.1; Fig. 3 and Table 3). During the cooler months
307 that are typically characterised by reduced *H. akashiwo* abundance, this inverse association *Mesodinium* and its
308 suspected prey was even more pronounced (t = -2.4 P < 0.05). An assessment of presence/absence, by
309 determining the median value during specified concentration ranges of co-occurring phytoplankton classes,
310 suggests that *M*. cf. *rubrum* is most likely to co-exist with higher abundances of taxa belonging to
311 Bacillariophyceae, Chlorodendrophyceae, Dinophyceae, and Euglenophyceae (Fig. 3).
312

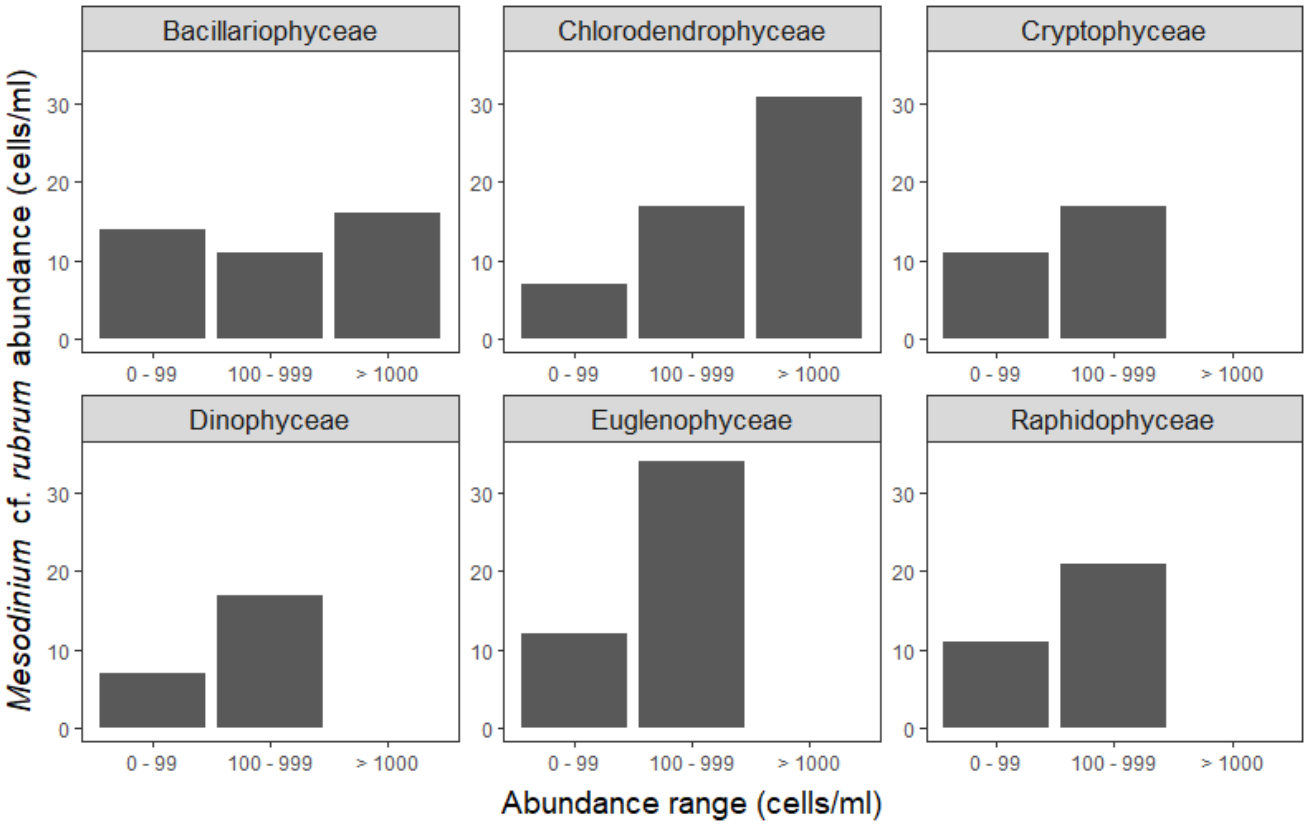

313

314 **Figure 3.** Median abundance of *M.* cf. *rubrum* during specified cell abundance ranges of co-occurring phytoplankton

315 classes (for variability estimates, refer to Table 2). Euglenophyceae abundance did not exceed 1,000 cells/ml during the

316 study period.

317

Table 3. Generalised least squares (GLS) model for overall *Mesodinium* abundance (cells ml^{-1}) across multiple sampling locations at the Sundays Estuary, South Africa from April 2018 to November 2019 (n = 204 sites sampled). The most-parsimonious model (AIC = 8757.4) included 'season' as a random residual variance (var) structure and sampling 'date' as an autocorrelation structure. The predictors fitted to this overall model were also fitted to separate seasonal models for only spring or summer (n = 551 samples) and autumn or winter (n = 244 samples). Non-factorial predictor variables are scaled and the coefficients (± standard error, SE) of those that are factors ('season', 'diel cycle', 'depth', and 'diel:depth' interaction) are presented relative to their reference categories, namely: 'autumn', 'day', '0 m' and 'day:0 m', respectively. The significance of the intercept as well as factor variables are tested using the 'anova' F-statistic and all other predictors using the 'summary' t-value of the 'nlme' package (Pinheiro et al. 2018), with: °P < 0.1, *P < 0.05; **P < 0.01; ***P < 0.001.

	Overall					*Spring/Summer*					*Autumn/Winter*				
Predictor	**C**	**SE**	**t/F**	**p**	**var**	**C**	**SE**	**t/F**	**p**	**var**	**C**	**SE**	**t/F**	**p**	**var**
Intercept	19.9	11.7	78.9	***		40.1	10.1	54.9	***		31.8	11.5	35.7	***	
Season			3.8	**				0.3	0.6				1.3	0.3	
SPRING	27.7	12.5	2.2	*	1.1										
SUMMER	37.0	19.6	1.9	°	1.4	4.9	18.0	0.3	0.8	1.3					
WINTER	-10.4	12.7	-0.8	0.4	0.7						-6.0	12.0	-0.5	0.6	0.7
Diel cycle			1.1	0.3				0.9	0.3				4.5	*	
NIGHT	-9.5	9.7	-1.0	0.3		-8.2	13.6	-0.6	0.5		-14.6	14.1	-1.0	0.3	
Depth			9.9	***				3.9	**				6.3	***	
0.5 m	15.7	6.7	2.4	*		19.8	9.2	2.2	*		16.9	9.9	1.7	°	
1.0 m	18.3	7.7	2.4	*		5.3	9.9	0.5	0.6		43.2	12.3	3.5	***	
BOTTOM	-19.1	8.6	-2.2	*		-22.4	10.9	-2.1	*		-3.9	14.1	-0.3	0.8	
Diel:depth			2.2	°				3.4	*				2.1	0.1	
NIGHT:0.5 m	-8.8	9.6	-0.9	0.4		-14.3	13.0	-1.1	0.3		-6.6	14.4	-0.5	0.6	
NIGHT:1.0 m	-2.4	10.8	-0.2	0.8		21.7	14.5	1.5	0.1		-33.9	16.5	-2.0	*	
NIGHT:BOTTOM	18.4	10.6	1.7	°		32.2	14.7	2.2	*		-1.7	15.8	-0.1	0.9	
Phytoplankton Biomass	10.6	3.5	3.0	**		13.4	5.1	2.6	**		8.6	5.3	1.6	0.1	
Raphidophyceae	-6.5	3.0	-2.2	*		-9.4	3.9	-2.4	*		-4.1	5.2	-0.8	0.4	
Cryptophyceae	-3.4	1.9	-1.8	°		6.2	3.6	1.7	°		-8.9	3.7	-2.4	*	
Salinity	9.3	3.9	2.4	*		3.3	5.6	0.6	0.6		12.0	5.9	2.1	*	
Salinity Stratification	10.8	4.1	2.7	**		22.4	5.6	4.0	***		0.1	4.9	0.0	1.0	
Temperature Stratification	6.2	4.4	1.4	0.2		10.5	5.8	1.8	°		-3.0	6.6	-0.5	0.7	
Dissolved Oxygen	5.7	3.7	1.5	0.1		7.0	5.0	1.4	0.2		8.8	6.5	1.3	0.2	
pH	-13.7	4.8	-2.8	**		-16.6	5.8	-2.9	**		-12.3	6.1	-2.0	*	
Phosphate	5.0	3.7	1.4	0.2		3.1	4.5	0.7	0.5		11.4	5.1	2.2	*	

4. Discussion

Identifying the drivers shaping phytoplankton population dynamics is complex due to the varying interactions between abiotic and biotic processes across timescales (Hall et al., 2015; Qin and Shen, 2017; Lemley et al., 2018a). Such understanding is critical to discerning phytoplankton species responses related to anthropogenic stressors (e.g. eutrophication, hydrological modifications) compared to natural processes. Specific to HABs becoming prevalent and widely distributed globally, mostly due to the amplification of anthropogenic nutrient loading, autecological studies help to discern other influences such as global change and natural population dynamics (Glibert, 2017, 2020). In the Sundays Estuary, seasonal temperature fluctuations are the only consistent natural abiotic process (i.e. flow variability is hindered by upstream diversion). This results in an ecosystem where the effects of anthropogenic stressors reflect clearly as high inorganic nutrient availability (~nitrate), distinct salinity stratification profiles (vertical and longitudinal), and increased water residency (Lemley et al., 2017). This uncharacteristic ecosystem stability and predictability provided a unique opportunity to explore the factors responsible for shaping the autecology of an otherwise well-studied HAB species, *Mesodinium* cf. *rubrum*.

Physical mixing patterns in the Sundays Estuary are driven by semi-diurnal tides, the spring-neap tidal cycle (range: 0.1 to 1.5 m; tidal prism: 0.6 to 2.2 x 10^6 m^3), and freshwater inflows. The estuary can be subdivided into four longitudinal sections according to predominant circulation patterns (*sensu* MacKay and Schumann, 1990): (1) well-mixed mouth inlet, (2) partially-mixed poly- to mixoeuhaline lower reaches (~40% of samples), (3) highly-stratified meso- to polyhaline middle reaches (~55% of samples), and (4) well-mixed oligohaline upper reaches (~5% of samples) with consistent seaward flow. Additionally, the effect of wind-mixing has been shown to be negligible (i.e. limited to surface layer, < 0.5 m depth), with distinct vertical haloclines persisting during strong wind events. Historically, the residence time of the system was estimated at seven neap tidal cycles and two spring cycles, with well-mixed conditions and little to no vertical stratification observed during spring tides. In recent times, elevated and consistent freshwater inflow volumes (i.e. water transfer scheme, irrigation return flows) have resulted in a loss of this well-mixed state. As such, the majority of the estuary now exhibits stratified

conditions with distinct haloclines (~excluding the upper reaches) during ebb and flood tides, regardless of diel (Lemley et al., 2018a) and spring-neap tidal cycles (Kotsedi et al., 2012; Lemley et al., 2017). Thermal gradients typically mirror salinity circulation patterns, and thus become less pronounced in spring and autumn when the temperature of inflowing seawater and freshwater are similar. The depth of the mixing layer, which persists year-round, varies between 0.5 and 1 m (mean, ca. 0.8 m; MacKay and Schumann, 1990), becoming shallower towards the mouth due to entrainment across the halocline between outflowing surface waters and high-salinity bottom waters.

As observed in other localities (Crawford and Lindholm, 1997; Crawford et al., 1997; Herfort et al., 2011a; Johnson et al., 2013), the abundance of *M*. cf. *rubrum* in the Sundays Estuary was closely linked to salinity and water column stability. Accordingly, "bloom" concentrations (> 100 cells ml^{-1}) were generally observed in polyhaline regions (> 18) of the estuary that exhibited pronounced salinity differences (> 10) between top and bottom-waters. This observation highlights the broad salinity ranges in which *M*. *rubrum* can proliferate, with studies in Chesapeake Bay (Johnson et al., 2013) and the Southampton Water Estuary (Crawford et al., 1997) demonstrating abundance maxima in mesohaline (< 10) and near-mixoeuhaline (> 28) waters, respectively. Aligned with previous observations, this study highlighted distinct vertical salinity stratification gradients as a key abiotic factor supporting accumulations of *M*. cf. *rubrum*. Thermal density gradients were less important in shaping these communities, with spring/summer *Mesodinium* populations marginally preferring the less dense thermoclines (cooler surface waters) associated with spring. This association with stratified conditions is complemented by the vertical migration capabilities of *M*. cf. *rubrum* which allow it to avoid horizontal displacement (Crawford and Purdie, 1992; Crawford and Lindholm, 1997; Fenchel and Hansen, 2006). Model results emphasized the distinct DVM patterns of this species through the water column in the highly stratified waters of Sundays Estuary (Table 3). *Mesodinium* cf. *rubrum* populations were most densely concentrated above (~0.5 m) or near (~1 m) the mixing layer during day-time periods and subsequently migrated to the bottom-waters at night. This positioning facilitates phased migration with the tidal and diel cycles to (1) limit advective losses (Crawford and Purdie, 1992; Hall et al., 2015) and (2) enable access to abundant surface and bottom water nutrient reservoirs (Lemley et al., 2017). The omittance of NO_x and ammonium as possible predictors during

383 model formulation in this study, together with a weak positive correlation with phosphate, highlight the non-
384 limiting nature of these variables on the growth of *M*. cf. *rubrum* in the Sundays Estuary.
385
386 Seasonality was also identified as an important predictor of *M*. cf. *rubrum* abundance in the Sundays Estuary,
387 with peak concentrations and variability occurring in summer and spring. This observation aligns well with
388 existing literature that has indicated the recurrent nature of *M. rubrum* red-water events in summer (Crawford et
389 al., 1997; Herfort et al., 2011a, 2011b) and spring (Johnson et al., 2013). However, the exclusion of water
390 temperature as a predictor in the univariate model and the occurrence of relatively high abundances (> 500 cells
391 ml^{-1}; Fig. 1) in winter suggests that other seasonally distinct variables are responsible for this temporal trend.
392 This is supported by previous reports of *M*. cf. *rubrum* maxima during winter (> 700 cells ml^{-1}) in the Sundays
393 Estuary (Lemley et al., 2018a). Therefore, the seasonal response of *M*. cf. *rubrum* detected in this study may be a
394 function of suitable prey availability; an observation supported by the inverse association highlighted between
395 *M*. cf. *rubrum* and Cryptophyceae abundance (Table 3). This relationship highlights the top-down grazing
396 pressure exerted by *Mesodinium* on its cryptophyte prey. Yet, the absence of any *M*. cf. *rubrum* red-water
397 accumulations (> 1,000 cells ml^{-1}) in the Sundays Estuary suggests that Cryptophyceae abundance (i.e. mean <
398 300 cells ml^{-1}; Table 2) may be insufficient to support HABs of these populations. This contrasts with a study by
399 Johnson et al. (2013) that reported mean cryptophyte concentrations in excess of 1,400 cells ml^{-1} in Chesapeake
400 Bay, an estuary known to support HAB formations of *M. rubrum* (max. 3,300 cells ml^{-1}). The continuous
401 reliance on suitable cryptophyte prey (TPG clade) to obtain organelles (e.g. nuclei, chloroplasts) and facilitate
402 acquired phototrophy has been well documented (Johnson, 2007; Herfort et al., 2011b; Peterson et al., 2013;
403 Johnson et al., 2016; Peltomaa and Johnson, 2017; Nishitani and Yamaguchi, 2018). During this study, the
404 inverse association between *M*. cf. *rubrum* and its potential cryptophyte prey was most pronounced during
405 winter and autumn. However, Cryptophyceae typically exhibit a strong preference ($P < 0.01$) for warm
406 conditions in the Sundays Estuary (Lemley et al., 2017), thus, potentially indicating a temporal mismatch in
407 suitable growing conditions between prey and consumer populations. Despite the predominantly limiting nature
408 of prey resources in the system, a high-biomass bloom event (> 100 µg Chl-*a* l^{-1}) of *Plagioselmis*
409 *nannoplanctica*, belonging to the TPG clade of cryptophytes, was recorded during late-winter (i.e. August 2018)

410 in this study. Interestingly, the abundance of *M*. cf. *rubrum* exhibited marked increases (*ca*. 650 cells ml^{-1})
411 approximately a month after this event in early-spring. Previous studies have highlighted rapid prey ingestion
412 rates by *M. rubrum*, reported to range from 4 to 12 cryptophytes d^{-1}, with the capture of a single cryptophyte cell
413 per day enough to sustain maximum growth rates (Hansen et al., 2013; Peltomaa and Johnson, 2017). As such,
414 *Mesodinium* populations (1) rapidly capture and assimilate organelles upon encountering high TPG cryptophyte
415 prey concentrations, and (2) alter planktonic food-web structures in the Sundays Estuary by restricting TPG
416 cryptophyte abundance. Notably, however, this accumulation of *M*. cf. *rubrum* in response to increased prey
417 availability coincided with the growing season of the resident HAB-forming species, *Heterosigma akashiwo*.
418
419 The absence of *M*. cf. *rubrum* populations at the onset of extensive HAB events (> 100 µg Chl-*a* l^{-1}) provides
420 insight into its limited bloom-forming potential in the Sundays Estuary. The interaction primarily responsible for
421 this is the strongly inverse association (see Table 3) between the abundance of *H. akashiwo* and *M*. cf. *rubrum*.
422 The success of *H. akashiwo* in the Sundays Estuary has been attributed to its physiological adaptions to
423 increased water temperatures (spring/summer), high photosynthetic efficiency (up to 20 chloroplasts $cell^{-1}$),
424 ability to rapidly assimilate inorganic nutrients, and highly motile nature that enables asynchronous DVM
425 behaviour (Lemley et al., 2017, 2018a, 2018b). These selective advantages facilitate extensive HAB events,
426 often exceeding 500 µg Chl-*a* l^{-1}, that have been shown to shape the abiotic environment during these periods,
427 e.g. nitrate and phosphate depletion (0 µM), elevated pH (> 9), bottom-water hypoxia (< 2 mg l^{-1}), and super-
428 saturated oxygen conditions (max. 19.7 mg l^{-1}). Accordingly, the affinity of *M*. cf. *rubrum* populations for less
429 extreme environmental conditions, i.e. less basic (pH < 9) and stable dissolved oxygen (5–9 mg l^{-1}) conditions,
430 highlight its apparent inability to persist and compete for resources during extensive HAB events of *H.*
431 *akashiwo*. Niche overlap between these two species is evident given that they share similar habitat preferences
432 (stratified and meso- to polyhaline waters), resource growth requirements (N and P), and species traits (~high
433 motility and associated DVM ability). Yet, in this study, the high frequency of near-monospecific HAB events of
434 *H. akashiwo* (*n* = 14), together with the additional constraint of requiring suitable cryptophyte prey
435 concentrations, culminated in *M*. cf. *rubrum* being outcompeted during otherwise favourable conditions in the
436 Sundays Estuary. It is also possible that the high pH conditions caused by *H. akashiwo* proliferations may further

437 inhibit *Mesodinium* populations by rendering a portion of available ammonium stocks (~preferred N source;
438 Crawford et al., 1997) as unattainable (i.e. speciation to ammonia gas). The exclusion of Dinophyceae as a
439 predictor from the most-parsimonious model in this study can, in part, be attributed to the absence of *Dinophysis*
440 species from the Sundays Estuary plankton community. Numerous species belonging to this genus are known to
441 facilitate their own acquired phototrophic behaviour through capturing ciliate prey, particularly *M. rubrum*
442 (Hansen et al., 2013 and references therein). The lack of any further associations between *M.* cf. *rubrum* and
443 other phytoplankton classes recorded in this study, suggests an ability to co-exist with taxa belonging to these
444 classes during intermediate bloom periods (> 5 but < 60 µg Chl-*a* l^{-1}). Therefore, despite potential niche overlap,
445 *Mesodinium* co-occurred with less abundant and motile phytoflagellates belonging to Chlorodendrophyceae (e.g.
446 *Tetraselmis* sp.), Dinophyceae (e.g. *Heterocapsa rotundata*), and Euglenophyceae (e.g. *Euglena* sp.). Similar
447 patterns of co-existence were observed with species belonging to Bacillariophyceae, although this is perhaps a
448 function of niche differentiation whereby ciliates occupy the entire water column, while diatom taxa (e.g.
449 *Pleurosigma angulatum*, *Cylindrotheca closterium*) are largely confined to areas below the mixing layer (halo-
450 and thermocline, i.e. > 1 m depth). Such niche partitioning has been proposed as an important ecological feature
451 that may provide refugia to higher trophic levels during HAB events in the Sundays Estuary (Lemley et al.,
452 2018a).
453
454 Perhaps most pertinently, this research documents the suppressive effects of frequent and high-magnitude HAB
455 events on *M.* cf. *rubrum* populations in temperate estuaries. The Sundays Estuary is also prone to high-biomass
456 winter HABs of *H. rotundata* (Lemley et al., 2017). This species, together with *H. akashiwo*, was first recorded
457 in the Sundays Estuary in the late 1980s (Hilmer and Bate, 1991) and coincided with the intensification of
458 upstream agricultural activities. Thus, in a scenario where these HABs continue to intensify (e.g. Kotsedi et al.,
459 2012; Lemley et al., 2017), it is likely that the abundance of *Mesodinium* populations will become further
460 constrained into the future. From a management perspective, it is critical that hydrodynamic variability is
461 reintroduced to the Sundays Estuary to restore an element of unpredictability to the phytoplankton community.
462 Examples of such interventions include the reclamation of nutrient-rich irrigation return flows and scheduled
463 dam releases (Lemley et al., 2018b). These measures would serve to provide a temporarily balanced

phytoplankton community, reducing HAB instances in the system and minimising the effects thereof, e.g. hypoxia, shading of submerged vegetation, and suffocation of faunal communities (~*H. akashiwo* mucilage production). As an example, the nearby Gamtoos Estuary shares key similarities with the Sundays Estuary (e.g. constant nutrient-rich baseflows, distinct salinity gradients), yet the natural flow variability it experiences has culminated in an ecosystem exhibiting only sporadic eutrophic symptoms (e.g. HABs, hypoxia) (Lemley et al., 2017). Interestingly, these dynamic conditions support increased abundance of Cryptophyceae in the Gamtoos Estuary. Thus, by mimicking natural flow variations in the Sundays Estuary, it could be expected that *M*. cf. *rubrum* populations would be better equipped to thrive, given a hypothesised reduction in HAB frequency and increased availability of cryptophyte prey.

5. Acknowledgements

This work is based on the research supported in part by the National Research Foundation (NRF) of South Africa (Grant Numbers: 120709) that provided funding to the lead author, Dr Daniel A. Lemley. Additionally, the DSI/NRF Research Chair in Shallow Water Ecosystems is acknowledged for providing the necessary funding to undertake field surveys and laboratory analyses. The authors would also like to thank Ms Patricia Smailes for assisting with the enumeration and identification of phytoplankton, and Mr Eugin Bornman for contributing greatly to sample collection. Finally, the RCUK-NRF Newton Fund is thanked for funding a research exchange programme that facilitated collaborative visits between Dr Daniel Lemley and co-author, Prof. Duncan Purdie at the University of Southampton, United Kingdom.

6. References

Adams, J.B., Taljaard, S., van Niekerk, L., Lemley, D.A., 2020. Nutrient enrichment as a threat to the ecological resilience and health of South African microtidal estuaries. Afr. J. Aquat. Sci. 45, 23–40.

490 Altenburger, A., Cai, H., Li, Q., Drumm, K., Kim, M, Zhu, Y., Garcia-Cuetos, L., Zhan, X., Hansen, P.J., John,
491 U., Li, S., Lundholm, N., 2020. Limits to the cellular control of sequestered cryptophyte prey in the marine
492 ciliate *Mesodinium rubrum*. bioRxiv, doi: https://doi.org/10.1101/2020.07.14.202424.
493
494 Anderson, D.M., 2009. Approaches to monitoring, control and management of harmful algal blooms (HABs).
495 Ocean Coast. Manage. 52, 342–347.
496
497 Bate, G.C., Heelas, B.V., 1975. Studies on the nitrate nutrition of two indigenous Rhodesian grasses. J. Appl.
498 Ecol. 12, 941–952.
499
500 Cloern, J.E., Abreu, P.C., Carstensen, J., Chauvaud, L., Elmgren, R., Grall, J., Greening, H., Johansson, J.O.R.,
501 Kahru, M., Sherwood, E.T., Xu, J., Yin, K., 2016. Human activities and climate variability drive fast-paced
502 change across the world's estuarine–coastal ecosystems. Glob. Change Biol. 22, 513–529.
503
504 Cole, B.E., Cloern J.E., 1987. An empirical model for estimating phytoplankton productivity in estuaries. Mar.
505 Ecol. Prog. Ser. 36, 299–305.
506
507 Coulon, C., Alexander, V., 1972. A sliding-chamber phytoplankton settling technique for making permanent
508 quantitative slides with applications in fluorescent microscopy and autoradiography. Limnol. Oceanogr. 17, 149–
509 152.
510
511 Crawford, D.W., 1989. *Mesodinium rubrum*: the phytoplankter that wasn't. Mar. Ecol. Prog. Ser. 58, 161–174.
512
513 Crawford, D.W., Lindholm, T., 1997. Some observations on vertical distribution and migration of the
514 phototrophic ciliate *Mesodinium rubrum* (= *Myrionecta rubra*) in a stratified brackish inlet. Aquat. Microb. Ecol.
515 13, 267–274
516

Crawford, D.W., Purdie, D.A., 1992. Evidence for avoidance of flushing from an estuary by a planktonic phototrophic ciliate. Mar. Ecol. Prog. Ser. 79, 259–265

Crawford, D.W., Purdie, D.A., Lockwood, A.P.M., Weissman, P., 1997. Recurrent red-tides in the Southampton Water Estuary caused by the phototrophic ciliate *Mesodinium rubrum*. Est. Coast. Shelf Sci. 45, 799–812.

Fenchel, T., Hansen, P.J., 2006. Motile behaviour of the bloom-forming ciliate *Mesodinium rubrum*. Mar. Biol. Res. 2, 33–40.

Glibert, P.M., 2017. Eutrophication, harmful algae and biodiversity – challenging paradigms in a world of complex nutrient changes. Mar. Poll. Bull. 124, 591–606.

Glibert, P.M., 2020. Harmful algae at the complex nexus of eutrophication and climate change. Harmful Algae 91, 101583.

Gustafson, D.E., Stoecker, D.K., Johnson, M.D., van Heukelem, W.F., Sneider, K., 2000. Cryptophyte algae are robbed of their organelles by the marine ciliate *Mesodinium rubrum*. Nature 405, 1049–1052.

Hall, N.S., Whipple, A.C., Paerl, H.W., 2015. Vertical spatio-temporal patterns of phytoplankton due to migration behaviors in two shallow, microtidal estuaries: Influence of phytoplankton function and structure. Est. Coast. Shelf Sci. 162, 7–21.

Hansen, P.J., Nielsen, L.T., Johnson, M., Berge, T., Flynn, K.J., 2013. Acquired phototrophy in *Mesodinium* and *Dinophysis* – A review of cellular organization, prey selectivity, nutrient uptake and bioenergetics. Harmful Algae 28, 126–139.

543 Herfort, L., Peterson, T.D., Campbell, V., Futrell, S., Zuber, P., 2011a. *Myrionecta rubra* (*Mesodinium rubrum*)
544 bloom initiation in the Columbia River estuary. Est. Coast. Shelf Sci. 95, 440–446.
545
546 Herfort, L., Peterson, T.D., McCue, L.A., Crump, B.C., Prahl, F.G., Baptista, A.M., Campbell, V., Warnick, R.,
547 Selby, M., Roegner, G.C., Zuber, P., 2011b. *Myrionecta rubra* population genetic diversity and its cryptophyte
548 chloroplast specificity in recurrent red tides in the Columbia River estuary. Aquat. Microb. Ecol. 62, 85–87.
549
550 Herfort, L., Peterson, T.D., Prahl, F.G., McCue, L.A., Needoba, J.A., Crump, B.C., Roegner, G.C., Campbell,
551 V., Zuber, P., 2012. Red waters of *Myrionecta rubra* are biogeochemical hotspots for the Columbia River
552 Estuary with impacts on primary/secondary productions and nutrient cycles. Estuar. Coast. 35, 878–891.
553
554 Hilmer, T., Bate, G.C., 1991. Vertical migration of a flagellate-dominated bloom in a shallow South African
555 estuary. Botanica Marina 34, 113–121.
556
557 Johnson, M.D., 2011. Acquired phototrophy in ciliates: a review of cellular interactions and structural
558 adaptations. J. Eukaryot. Microbiol. 58, 185–195.
559
560 Johnson, M.D., Beaudoin, D.J., Laza-Martinez, A., Dyhrman, S.T., Fensin, E., Lin, S., Merculief, A., Nagai, S.,
561 Pompeu, M., Setälä, O., Stoecker, D.K., 2016. The genetic diversity of *Mesodinium* and associated cryptophytes.
562 Front. Microbiol. 7, 2017.
563
564 Johnson, M.D., Oldach, D., Delwiche, C.F., Stoecker, D.K., 2007. Retention of transcriptionally active
565 cryptophyte nuclei by the ciliate *Myrionecta rubra*. Nature 445, 426–428.
566
567 Johnson, M.D., Stoecker, D.K., Marshall, H.G., 2013. Seasonal dynamics of *Mesodinium rubrum* in Chesapeake
568 Bay. J. Plankt. Res. 35, 877–893.
569

570 Kim, M., Park, M.G., 2019. Unveiling the hidden genetic diversity and chloroplast type of marine benthic ciliate
571 *Mesodinium* species. Sci. Rep. 9, 14081.
572
573 Kotsedi, D., Adams, J.B., Snow, G.C., 2012. The response of microalgal biomass and community composition to
574 environmental factors in the Sundays Estuary. Water SA 38, 177–190.
575
576 Lasek-Nesselquist, E., Wisecaver, J.H., Hackett, J.D., Johnson, M.D., 2015. Insights into transcriptional changes
577 that accompany organelle sequestration from the stolen nucleus of *Mesodinium rubrum*. BMC Genomics 16,
578 805.
579
580 Lemley, D.A., Adams, J.B., Rishworth, G.M., 2018a. Unwinding a tangled web: a fine-scale approach towards
581 understanding the drivers of harmful algal bloom species in a eutrophic South African estuary. Estuar. Coast. 41,
582 1356–1369.
583
584 Lemley, D.A., Adams, J.B., Strydom, N.A., 2018b. Triggers of phytoplankton bloom dynamics in permanently
585 eutrophic waters of a South African estuary. Afr. J. Aquat. Sci. 43, 229–240.
586
587 Lemley, D.A., Adams, J.B., Taljaard, S., 2017. Comparative assessment of two agriculturally-influenced
588 estuaries: similar pressure, different response. Mar. Poll. Bull. 117, 135–146.
589
590 Lindholm, T., 1985. *Mesodinium rubrum* - a unique photosynthetic ciliate. Adv. Aquat. Microbiol. 3, 1–48.
591
592 MacKay, H.M., Schumann, E.H., 1990. Mixing and circulation in the Sundays River Estuary, South Africa. Est.
593 Coast. Shelf Sci. 31, 203–136.
594
595 Moeller, H.V., Johnson, M.D., 2018. Preferential plastid retention by the acquired phototroph *Mesodinium*
596 *chamaeleon*. J. Eukaryot. Microbiol. 65, 148–158.

Nishitani, G., Yamaguchi, M., 2018. Seasonal succession of ciliate *Mesodinium* spp. with red, green, or mixed plastids and their association with cryptophyte prey. Sci. Rep. 8, 17189.

Nusch, E.A., 1980. Comparison of different methods for chlorophyll and phaeopigment determination. Archiv für Hydrobiologie 14, 14–36.

Paerl, H.W., Hall, N.S., Peierls, B.L., Rossignol, K.L., 2014. Evolving paradigms and challenges in estuarine and coastal eutrophication dynamics in a culturally and climatically stressed world. Estuar. Coast. 37, 243–258.

Parsons, T.R., Maita, Y., Lalli, C.M., 1984. A manual of chemical and biological methods for seawater analysis. New York: Pergamon Press.

Peltomaa, E., Johnson, M.D., 2017. *Mesodinium rubrum* exhibits genus-level but not species-level cryptophyte prey selection. Aquat. Microb. Ecol. 78, 147–159.

Pereira, P., Botelho, M.J., Cabrita, M.T., Vale, C., Moita, M.T., Gonçalves, C., 2012. Winter–summer nutrient composition linkage to algae-produced toxins in shellfish at a eutrophic coastal lagoon (Óbidos lagoon, Portugal). Est. Coast. Shelf Sci. 112, 61–72.

Peterson, T.D., Golda, R.L., Garcia, M.L., Li, B., Maier, M.A., Needoba, J.A., Zuber, P., 2013. Associations between *Mesodinium rubrum* and cryptophyte algae in the Columbia River estuary. Aquat. Microb. Ecol. 68, 117–130.

Pinheiro, J., Bates, D., DebRoy, S., Sarkar, D., R Core Team., 2018. nlme: Linear and nonlinear mixed effects models. In: R package version 3.

624 Qin, Q., Shen, J., 2017. The contribution of local and transport processes to phytoplankton biomass variability
625 over different timescales in the Upper James River, Virginia. Est. Coast. Shelf Sci. 196, 123–133.
626
627 R Core Team., 2020. R: A language and environment for statistical computing. In. Vienna, Austria: R
628 Foundation for Statistical Computing.
629
630 Snow, G.C., Bate, G.C., Adams, J.B., 2000. The effects of a single freshwater release into the Kromme Estuary.
631 2: microalgal response. Water SA 26, 301–310.
632
633 Warwick, R.M., Tweedley, J.R., Potter, I.C., 2018. Microtidal estuaries warrant special management measures
634 that recognize their critical vulnerability to pollution and climate change. Mar. Poll. Bull. 135, 41–46.
635
636 Zuur, A.F., Ieno, E.N., Walker, N.J., Saveliev, A.A., Smith, G.M., 2009. Mixed effects models and extensions in
637 ecology with R. New York: Springer.
638
639 Zuur, A.F., Ieno, E.N., Elphick, C.S., 2010 A protocol for data exploration to avoid common statistical
640 problems. Methods Ecol. Evol. 1, 3–14.